Interfacial defects distribution and strain coupling in the vertically aligned nanocomposite $YBa_2Cu_3O_{7-X}$/ $BaSnO_3$ thin films

Yuanyuan Zhu, Chen-Fong Tsai, Jie Wang, Ji Heon Kwon, and Haiyan Wang[a)]
Department of Electrical and Computer Engineering, Texas A&M University, College Station, Texas 77843-3128

Chakrapani V. Varanasi, Jack Burke, and Lyle Brunke
University of Dayton Research Institute, Dayton, Ohio 45469

Paul N. Barnes
Air Force Research Laboratory, Wright-Patterson AFB, Ohio 45433

(Received 17 November 2011; accepted 26 March 2012)

In this article, we report the unique microstructural characteristics of $YBa_2Cu_3O_{7-x}$ (YBCO)/$BaSnO_3$ (BSO) nanocomposite thin films on $LaAlO_3$ (LAO) substrates. The BSO secondary phase grows as self-assembled vertically aligned nanopillars uniformly distributed in the superconducting YBCO matrix. Detailed microstructure and strain studies including x-ray diffraction, cross-section and plan-view transmission electron microscopy, and geometric phase analysis reveal that, as the BSO doping concentration varied from 2 mol% to 20 mol%, the nanopillar density increased from $0.26 \times 10^{11}/cm^2$ to $1.44 \times 10^{11}/cm^2$ while the diameter of the nanopillars remains relatively constant (7–8 nm in diameter). The strain state of the YBCO matrix is affected by both lateral and vertical lattice strains; while, the BSO lattice is strongly tuned by YBCO rather than the substrate. A high-density array of dislocations in the order of $10^{13}/cm^2$ was observed along the vertical heterogeneous interfaces throughout the YBCO film thickness for all doping concentrations.

I. INTRODUCTION

Since the first demonstration of the $La_{0.7}Ca_{0.3}MnO_3$:MgO nanocomposite system,[1] the two-phase nanocomposite thin films, holding the promise for multifunctionality, have drawn extensive research interests.[2–4] For example, the $BiFeO_3$ (BFO):$CoFe_2O_4$ (CFO) nanocomposites combine ferroelectric and magnetic properties together achieving multiferroic characteristics.[5] Following that, a unique family of two-phase nanocomposite with vertical lattice alignment, termed as the vertically aligned nanocomposites (VAN), has been demonstrated in several systems.[6,7] For example, the $La_{0.5}Sr_{0.5}CoO_3$ (LSCO):$Ce_{0.9}Gd_{0.1}O_{1.95}$ (CGO) VAN was fabricated as the interfacial layer between the cathode and the electrolyte and proven to effectively increase the cell efficiency in solid oxide fuel cells.[8] More interestingly, the strain coupling along the vertical lattice matched interfaces in VAN systems can be further tuned by the diameter and density of the nanopillars.[9,10] New functionality and unique strain coupling are attractive for future applications; however, fundamental study on the vertical lattice matching and the nature of the defects along the vertical interfaces is scarce in the literature.

On the other hand, in the field of high-temperature superconductors (HTS) such as $YBa_2Cu_3O_{7-}$(YBCO),[11] maintaining the critical current density J_c of the film under applied magnetic field, i.e., excellent in-field performance, is one of the major challenges for practical applications.[12] One of the main approaches is to introduce nanoscale defects in YBCO matrix, which serve as the flux-pinning centers under high fields.[12,13] These dopants have to be chemically compatible with YBCO and be capable of growing epitaxially in the YBCO matrix. Among all of the artificial pinning centers introduced including the 0D,[14] 1D,[15,16] and 2D[17] defects; to date, vertically aligned nanopillars are considered to be one of the most effective pinning schemes. For example, Goyal et al. showed a stronger pinning effect along c-axis for $BaZrO_3$ nanorods doped YBCO films.[18] Varanasi et al. demonstrated the $BaSnO_3$ (BSO)-doped YBCO films with significantly enhanced c-axis pinning effects.[19,20] Recently, Wee et al. chose Ba_2GdTaO_6[21] and Ba_2YNbO_6[22] which chemically and structurally similar to YBCO as the secondary phase, achieving self-assembled growth as well as flux pinning enhancement. However, the nature of the defects and the effects of the strain[23] along the vertical interfaces that could be responsible for superconductive performance are still under investigation.

In this work, we select BSO-doped YBCO films with different doping concentrations as the typical system to investigate the microstructural origin of the VAN growth

[a)]Address all correspondence to this author.
e-mail: wangh@ece.tamu.edu
DOI: 10.1557/jmr.2012.125

 © Materials Research Society 2012

https://doi.org/10.1557/jmr.2012.125 Published online by Cambridge University Press

and the nature of the defects along the heterogeneous interface in the systems. The reasons BSO-doped YBCO system is chosen for this study are (i) BSO nanopillars grow epitaxially in YBCO matrix over a large thickness range; and (ii) the BSO nanopillar density can be easily tuned over a wide range by controlling the doping concentration of BSO. A combination of cross-section and plan-view transmission electron microscopy (TEM) study was applied to all the VAN films with different doping concentrations for exploring the distribution and dimension of the BSO phases. The out-of-plane lattice strain and matching relation of YBCO and BSO were studied for exploring the possible growth mechanisms of the self-assembled BSO nanopillars.

II. EXPERIMENTAL

Depositions of YBCO thin films with different $BaSnO_3$ concentrations (2 mol%, 4 mol%, 10 mol%, and 20 mol%) were conducted using pulsed laser deposition (PLD). The ratio of YBCO to BSO in the resulting thin films was controlled by varying the amount of powders in the composite targets preparation. Starting with commercially available YBCO (Nexans, Hurth, Germany) and BSO powders (Cerac, Milwaukee, WI), which were carefully weighed and well mixed to achieve four final targets with 2 mol%, 4 mol%, 10 mol%, and 20 mol% BSO in YBCO, respectively. Then, four composite films, up to a thickness of approximately 300 nm, were obtained on (100) $LaAlO_3$ (LAO) single crystal substrates. The details on target processing and deposition details can be found elsewhere.[21]

A systematic microstructural characterization was conducted via x-ray diffractometer (XRD) and TEM. Plan-view and cross-section TEM samples were prepared through a conventional TEM sample preparation routine including cutting, gluing, grinding, polishing, and final precision ion polishing. The TEM characterization was performed using a Philips CM200F analytical electron microscope with a point-to-point resolution of 0.20 nm.

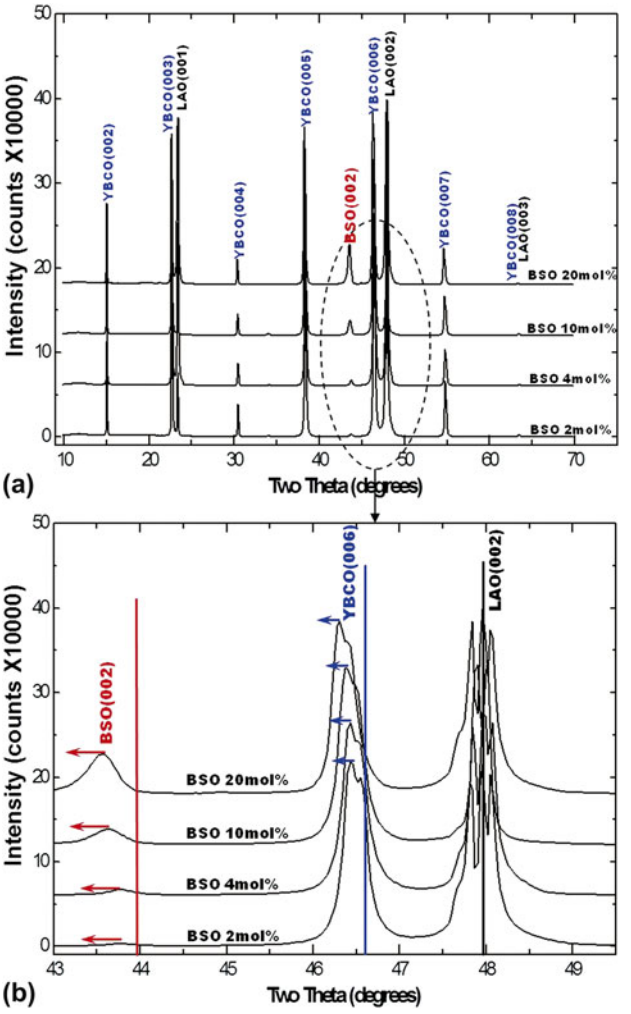


FIG. 1. XRD θ–2θ scans of YBCO samples with 2 mol%, 4 mol%, 10 mol%, and 20 mol% BSO in: (a) the full range; (b) the enlarged XRD scan showing YBCO (006) and BSO (002) peaks. All diffraction patterns are normalized with the strongest LAO (002) peak. The peak positions of bulk YBCO and BSO are noted in (b) as solid line for reference.

III. RESULTS AND DISCUSSION

The overall microstructure of the YBCO/BSO films was first characterized by XRD. In Fig. 1(a), all the films show primarily YBCO (00*l*) peaks and BSO (002) peaks in the typical θ–2θ scans, indicating that all four composite films are highly textured along YBCO (00*l*) on LAO (001) substrates. As the BSO concentration increased from 2 mol% to 20 mol%, the corresponding BSO (002) peak intensity also increased while no other peaks from other BSO orientations or other impurity phases were observed. This suggests that the primary (002) orientation remains as BSO doping concentration increases. Under this orientation relationship of YBCO(00*l*)//BSO(00*l*)//LAO(001), the theoretical lattice misfit rate, as well as corresponding coherent matching dislocation spacing and residual strains are calculated using the bulk lattice constants for the lateral and the vertical interface, respectively. As listed in Table I, in the epitaxial thin film, besides the conventional lateral lattice confinement from the substrate, a lattice misfit of ~5.535% between the two film phases–YBCO and BSO-is suggested. It is interesting to note that, as shown in the enlarged XRD pattern in Fig. 1(b) with all diffraction peaks normalized based on the strongest LAO (002) peak, both YBCO (006) and BSO (002) peaks shift toward lower angles, i.e., larger out-of-plane lattice parameters, as the BSO concentration increases. The ratio of YBCO (006)/(005) peak intensity was calculated for each sample and remained relatively constant. It indicates little or no variation in oxygen stoichiometry of the YBCO matrix for all the samples, which is in agreement with the fact that all

https://doi.org/10.1557/jmr.2012.125 Published online by Cambridge University Press

TABLE I. The list of theoretical in-plane and out-of-plane lattice misfit, dislocation spacing calculated by bulk lattice parameters at room temperature.

Theoretical predictions (assuming coherent contact)	Lateral (substrate) Strain LAO a_s = 3.789 Å		Vertical (matrix) Strain YBCO $c_0/3$ = 3.894 Å
	YBCO $\bar{a}_0$ = 3.852 Å	BSO a = 4.116 Å	BSO c = 4.116 Å
Bulk lattice misfit (%) $2(a_s\text{-}a_f)/(a_s + a_f)$	//: −1.649 YBCO in//compression	//: −8.273 BSO in//compression	⊥: −5.535 BSO in ⊥ compression
Dislocation spacing (nm) $d_{002s}d_{002f}/\lvert d_{002s}\text{-}\ d_{002f}\rvert$	11.584	2.385	3.704

Note: for the vertical strain prediction, the d_c(001) of YBCO is divided by three, i.e., the averaged $c/3$ = 3.894Å, for simplification. In the calculation of dislocation spacing, d_{002s} is adopted considering the actual (002) monolayer matching.

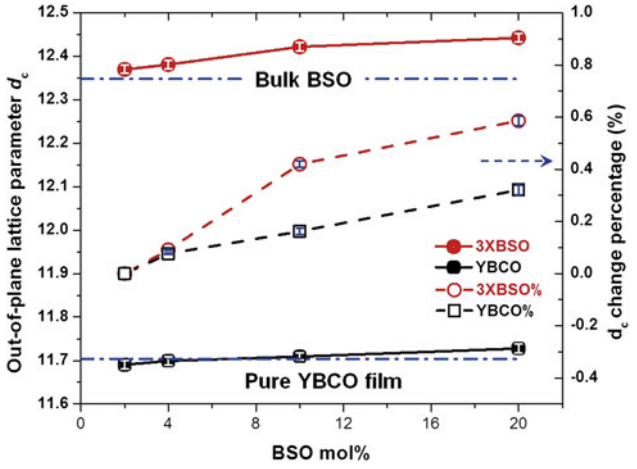


FIG. 2. The plot of XRD out-of-plane lattice parameter and corresponding percentage variations of the YBCO and the BSO in all four samples.

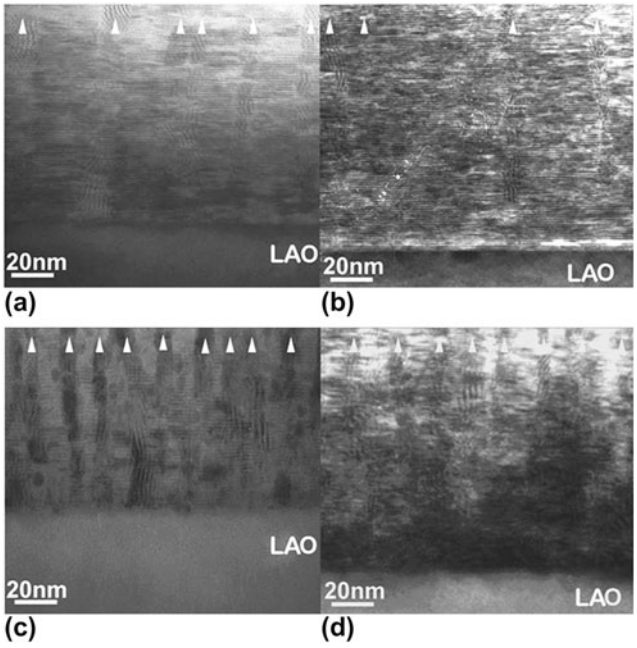


FIG. 3. Low magnification XTEM images of YBCO/BSO composites on LAO substrates with (a) 2 mol%, (b) 4 mol%, (c) 10 mol%, and (d) 20 mol% BSO, respectively. High-density vertically aligned BSO nanocolumns are cleared observed in all four samples and marked as white triangles.

of the films were prepared under the same PLD conditions. The calculated d_c of the YBCO matrix and of the BSO secondary phase, as well as their increases as a function of doping concentration is then presented in Fig. 2. Comparing to the d_c of a 280-nm-thick pure YBCO thin film (~11.704 Å), the out-of-plane d_c of the YBCO phase in the doped thin films only shows a very small variation. However, the d_c of the BSO secondary phase increases about 0.6% when the doping concentration rises to 20 mol%.

To explore how the BSO secondary phase disperses in the YBCO matrix and the related defects caused by the dopant structures, we conducted both plan-view and cross-section TEM (XTEM) studies on all the composite films. Figure 3 shows low magnification XTEM images of YBCO + BSO films on LAO substrates with BSO doping concentration varied from 2 mol% to 20 mol%. It is noted that nicely grown BSO nanopillars align vertically throughout the film thickness. With the increase of BSO concentration, these vertically aligned nanopillars were not growing wider; instead, their density increases accordingly. A clear illustration of the dimension and distribution of the BSO nanocolumns with different doping concentrations is presented in the plan-view TEM images in Fig. 4. As the BSO concentration increases from Fig. 4(a) 2 mol% to Fig. 4(d) 20 mol%, the nanopillars density increases from $2.60 \times 10^{10}/cm^2$ to $1.44 \times 10^{11}/cm^2$ while the diameter of the nanocolumns remained relatively constant at about 7–8 nm in diameter.

From the above XRD and TEM analysis, it is obvious that the YBCO + BSO films have grown as heteroepitaxial two-phase VAN. Different from most of the other artificial secondary phases, e.g., nanoparticles like $BaZrO_3$ (BZO)[16] and Y_2O_3[24] or nanolayers such as CeO_2[17,25] and Y_2BaCuO_6[14], the BSO continuous nanopillars in the VAN structure grew epitaxially and simultaneously with YBCO matrix through the film thickness. Based on the Winterbottom construction[26] and recently presented guidelines to the materials selection of the self-assembled vertical nanocomposites,[6] the intrinsic similarity in crystalline structures and out-of-plane lattice matching between the cubic Perovskite BSO and YBCO matrix, as well as the

https://doi.org/10.1557/jmr.2012.125 Published online by Cambridge University Press

comparable wetting ability to the surface of (001) pseudo-cubic LAO substrate for both phases, these developments indicate the tantalizing possibility of heteroepitaxy BSO in 3D (i.e., both in-plane as well as out-of-plane). Compared with another frequently used secondary addition—BZO—which forms continuous nanorods only under certain PLD conditions and many of the BZO nanorods were observed bent as film thickness increases;[27] BSO nanopillars intend to maintain the steady straight growth, despite our efforts in trying to break their continuity by raising deposition temperature during the PLD process. Thus, the proposed 3D heteroepitaxy was found to be quite robust in the PLD-grown BSO/YBCO system and also in other $REBa_2Cu_3O_y$ (RE: rare-earth element) films.[28] The detailed self-assembled growth dynamics and morphology control of the nanostructures have been studied as one of the fundamental issues of the self-assembled nanocomposites,[26] which are beyond the scope of this work. Here, we are trying to further investigate the lattice matching between the two phases that one occupies dominant film volume than the other; and to explore how they accommodate the challenge of an extra heterogeneous interface achieving the VAN structure.

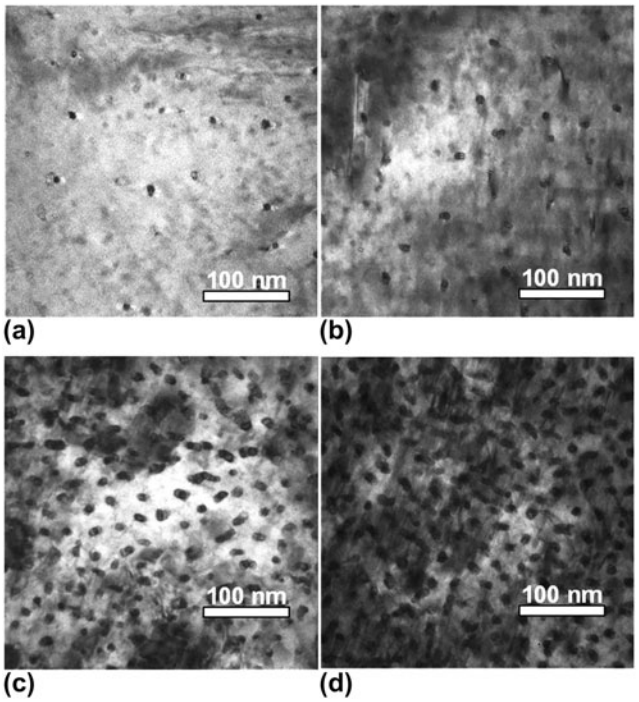


FIG. 4. Plan-view TEM micrographs of YBCO/BSO composites with (a) 2 mol%, (b) 4 mol%, (c) 10 mol%, and (d) 20 mol% BSO, respectively. The as-observed elliptic cross-sections of the BSO nanocolumns are due to an angle between the sample surface normal and the column axis. The diameter of the BSO nanocolumns was estimated from the shorter radius.

The strain state of the 300 nm-thick YBCO + BSO VAN film is determined by two competing factors, i.e., the lateral strain from the substrate and the vertical strain between the two phases. To determine which one is dominant, the ratios of the vertical to lateral interface areas for BSO and YBCO are listed in Table II, in 2 mol% and 20 mol% samples respectively. For BSO, apparently the vertical interface area between BSO and YBCO is much larger (about 150 times larger) than the lateral interface, due to the very small BSO nanopillar diameter. This suggests that the vertical strain is dominant in the BSO nanocolumns, and it seems unaffected by the doping concentration. According to the theoretical predications listed in Table I, since BSO has a larger c-lattice parameter of 4.116 Å than the c/3 of YBCO (3.894 Å), a large vertical compression (~5. 385%) is expected in BSO in the ideal coherent lattice matching. However, as shown in Fig. 5, the vertical BSO/YBCO interface observed in practice suggests otherwise. HRTEM images of the 4 mol% and 20 mol% samples, and their corresponding fast Fourier filtered images are shown in Figs. 5(a)–5(d), respectively. Along the interface between BSO and YBCO, localized dislocation-like contrast [marked as white "T" in Figs. 5(b) and 5(d)] was observed in both samples. Taking the 4 mol% sample for instance, the misfit dislocation spacing (d_M) measured here in Fig. 5(b) is only ~3 nm, indicating a domain matching epitaxy (DME)[29] where 14 of (002) BSO lattices match with 15 of (006)YBCO lattices. Under such matching condition, the residual strain in BSO yields a vertical tension ~1.3%. The same filtered Fast Fourier Transformation (FFT) was applied to the high-resolution TEM (HRTEM) images taken at the vertical interfaces from samples with different doping concentrations. Although it is not conclusive that the VAN film with higher BSO concentration has a smaller d_M, a d_M

TABLE II. Calculations of the vertical to lateral interface areas ratios of the BSO and the YBCO in the VAN films with 2 mol% and 20 mol% BSO, respectively.

BSO concentration	2 mol%	20 mol%
BSO nanocolumn density (per cm^2 of the film/sub interface)	2.60×10^{10}	1.44×10^{11}
BSO/Sub interface area (cm^2)	$\pi r^2 \times 2.60 \times 10^{10} = 1.31 \times 10^{-2}$	$\pi r^2 \times 1.44 \times 10^{11} = 7.23 \times 10^{-2}$
BSO/YBCO vertical interface area (cm^2)	$2\ \pi rh \times 2.60 \times 10^{10} = 1.96$	$2\ \pi rh \times 1.44 \times 10^{11} = 10.85$
Vertical interface area/Lateral interface area of BSO	$1.96/1.31 \times 10^{-2} = 10.85/7.23 \times 10^{-2} = 2\ h/r = 150$	
Vertical interface area/Lateral interface area of of YBCO	$1.96/1–1.31 \times 10^{-2} = 1.99$	$10.85/1–7.23 \times 10^{-2} = 11.70$

Note: r refers to the radius of the BSO nanocolumn which is about 4 nm measured by TEM; h = 300 nm is the film thickness.

https://doi.org/10.1557/jmr.2012.125 Published online by Cambridge University Press

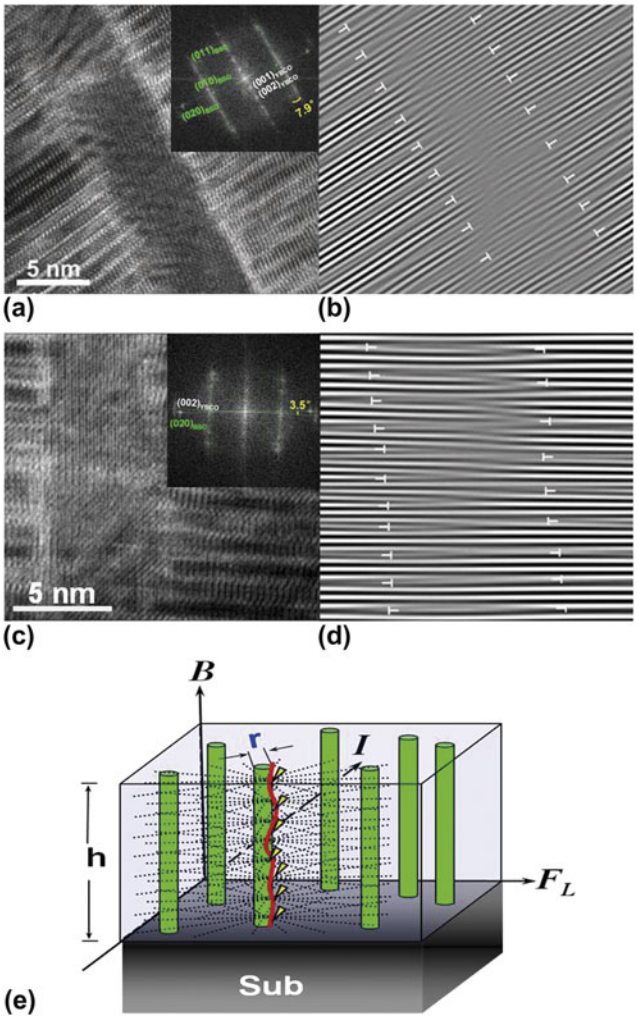


FIG. 5. TEM observations at the BSO-YBCO vertical interface and the schematic illustration of the flux-pinning effect of the vertical interfacial defects under applied magnetic fields. HR-XTEM images and corresponding filtered FFT images are shown in (a) and (b), (c), and (d) for the 4 mol% and 20 mol% film, respectively. Misfit dislocations are marked as white "T" along the vertical interface. In (e), the thickness of the YBCO thin film is noted as h; the radius of the nanopillar is noted as r, respectively. When transport current (I) is applied under the magnetic field (B), the resulting Lorentz force (F_L) moves vortices toward right (showing by curved vortices line in red), dissipating energy and causing the electric resistivity to occur. The vertical-interfacial-defects and their effects in pinning the vortices lines are illustrated in terms of the defects density. The misfit dislocation lines are noted as dotted lines around each doping phase.

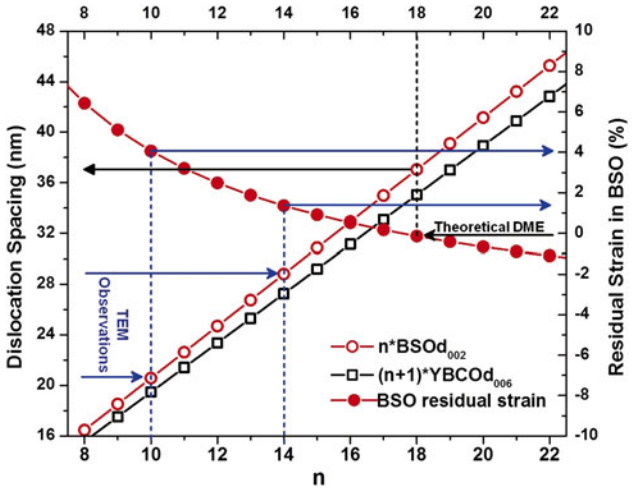


FIG. 6. The plots of the dislocation spacing and BSO residual strain variation as a function of the domain epitaxy matching n. Black arrows and dashed lines guide the view of theoretical domain matching epitaxy; blue lines guide the TEM observed matching results in the YBCO/BSO nanocomposite film. The practical dislocation spacing (or domain size), as shown, is smaller than the theoretical prediction, resulting in the reverse in the vertical strain state of BSO.

of ~2 nm, resulting in an even larger residual strain ~4% in BSO, is observed at a section of vertical interface in the 20 mol% sample. Based on the theoretically predicted dislocation spacing (Table I), the ideal dislocation spacing is ~3.7 nm, yielding a very small residual compression ~−0.05% in the BSO (as shown by the black arrows in Fig. 6). However, practically, the dislocation spacing along the vertical interface is smaller (2–3 nm) than the theoretically calculated value, as illustrated by blue arrows in Fig. 6. This modified DME, thus, introduces considerably large residual tension in the BSO.

Moreover, besides the above lattice extension/compression, local lattice rotation related to the tilting growth of the BSO nanopillars, is also observed in the VAN films, especially those with low BSO concentration. As shown in Fig. 7(a), a BSO nanopillar in a 4 mol% film has a ~6° tilt off the c-axis. It is surrounded by an amorphous-like area with a thickness of 2–3 unit cells (~2.5 nm). While in the samples with higher BSO doping concentrations, such as Fig. 7(b), a thinner amorphous region (~1 nm) is found mainly on the left side of a straighter BSO nanopillar in the 20 mol% sample. From our experience, the emerging of amorphous-like layers between YBCO and substrate could be introduced by TEM foil preparation. Whereas, these observed tilting growth is more likely attributed to the large lattice mismatch between BSO and LAO substrate (~−8.273%). Since YBCO competes with BSO during the initial film growth, it could be difficult for BSO to grow laterally and become wide enough to form domain matching epitaxy. One effective way of relieving this large lateral strain is tilting the BSO nanopillars slightly off the c-axis. And this titling growth could, in turn, impact the local out-of-plane and in-plane contact lattice relationship.

In all, a great number of dislocations with spacing 2–3 nm were observed along each BSO-YBCO vertical interface, and the dislocation density increases as the number of BSO nanopillar increases. Conventionally, interfacial defects, especially misfit dislocations, are of great interest in functional oxide thin films.[30] For example the film-substrate interfacial defects are believed to be responsible for the high J_c of YBCO and attribute to the thickness

https://doi.org/10.1557/jmr.2012.125 Published online by Cambridge University Press

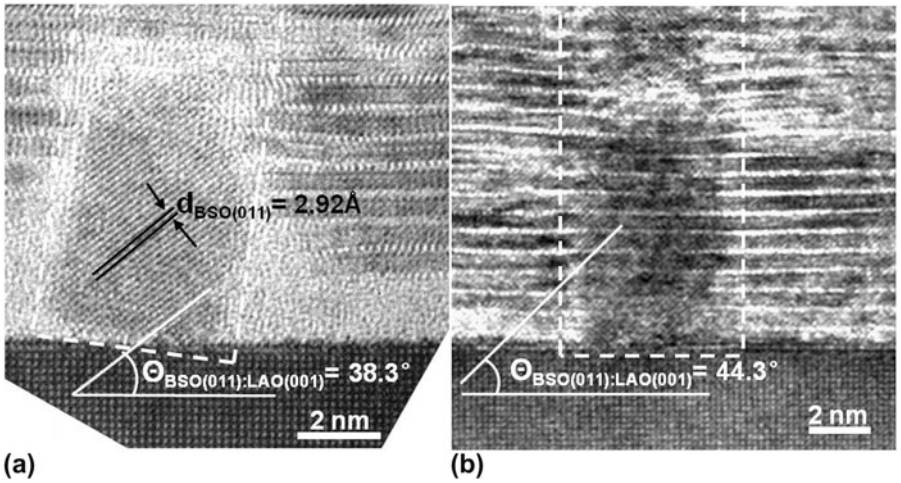


FIG. 7. The enlarged XTEM images of the film/substrate regions of the YBCO + BSO film with (a) 4 mol% and (b) 20 mol% BSO, respectively. The BSO nanopillars' tilting angles are characterized by the angle between the BSO(011) and LAO(001), which is 45° in idea case.

dependence effect of YBCO films.[31] For this BSO-YBCO VAN case, the BSO nanopillars as well as the defects along the interfaces between the BSO and YBCO are the effective pinning centers for the enhanced in-field performance.[19,20] A recent study on $BaZrO_3$ doped YBCO films (BZO/YBCO) shows that the strain induced oxygen stoichiometry variation along the interfaces could also affect YBCO's superconducting performance.[23] In the BSO/YBCO case, the T_c of YBCO maintains a high value of >87 K for all concentrations.[20] Therefore the effects of oxygen stoichiometry variation in the BSO/YBCO case might not be as strong as that in the BZO/YBCO case. A schematic illustration of the defect distribution and corresponding pinning effects of the VAN YBCO thin films is presented in Fig. 5(e). Under the applied magnetic field (B), the resulting Lorentz force (F_L) could move vortices toward right (illustrated by the red vortices' line), dissipating energy and causing the electric resistivity to occur. As illustrated here, the vertically aligned BSO nanopillars can provide the possibility of arranging the pinning centers throughout the YBCO film thickness and achieving a much stronger pinning effect especially for high-field applications. The above defects analysis and discussions agrees well with the J_c results measured in applied magnetic field,[20] which showed an obvious enhancement in $J_c^{in\text{-}field}$ (H//c) as the YBCO doped with higher BSO concentrations. Therefore, although the accurate control on the density of the vertical interfacial defect is complex, VAN configuration is a promising approach for introducing and, more importantly, distributing the flux-pinning defects throughout the film thickness and forms a 3D defect network.

IV. SUMMARY

In conclusion, we have conducted in-depth microstructural characterizations on the PLD-grown BSO/YBCO VAN to explore the growth mechanism and vertical strain tuning of VAN. In all four YBCO films with the BSO doping concentration varied from 2 mol% to 20 mol%, continuous BSO nanopillars with nearly constant diameters of around 7–8 nm, grow epitaxially and distribute randomly in the YBCO matrix. XRD results suggest a strong lattice strain tuning between the YBCO matrix and the doped BSO nanopillars as a function of the nanopillar density. It was noted that along their vertical heterogeneous interfaces, a high density of dislocations in the order of $10^{13}/cm^2$ is found throughout the YBCO film thickness. These high-density vertical interfacial defects could act as strong c-axis pinning centers and be responsible for the high-field performance of YBCO films regardless of the film thickness.

ACKNOWLEDGMENTS

This research was funded by the Air Force Office of Scientific Research (Contract No.: FA9550-09-1-0114), and AFRL–Propulsion Directorate. The TEM characterization effort was supported by National Science Foundation (NSF-0846504). J.H. Kwon was supported by the Undergraduate Summer Research program at Texas A&M University.

REFERENCES

1. O.I. Lebedev, J. Verbeeck, G. Van Tendeloo, O. Shapoval, A. Belenchuk, V. Moshnyaga, B. Damashcke, and K. Samwer: Structural phase transitions and stress accommodation in $(La_{0.67}Ca_{0.33}MnO_3)_{1-x}$:$(MgO)_x$ composite films. *Phys. Rev. B* **66**, 104421 (2002).
2. J. Ma, J.M. Hu, Z. Li, and C.W. Nan: Recent progress in multiferroic magnetoelectric composites: From bulk to thin films. *Adv. Mater.* **23**, 1062 (2011).

https://doi.org/10.1557/jmr.2012.125 Published online by Cambridge University Press

3. C.W. Nan, M.I. Bichurin, S.X. Dong, D. Viehland, and G. Srinivasan: Multiferroic magnetoelectric composites: Historical perspective, status, and future directions. *J. Appl. Phys.* **103**, 31101 (2008).
4. S.A. Harrington, J.H. Durrell, H. Wang, S.C. Wimbush, C.F. Tsai, and J.L. MacManus-Driscoll: Understanding nanoparticle self-assembly for a strong improvement in functionality in thin film nanocomposites. *Nanotechnology* **21**, 235702 (2010).
5. H. Zheng, J. Wang, S.E. Lofland, Z. Ma, L. Mohaddes-Ardabili, T. Zhao, L. Salamanca-Riba, S.R. Shinde, S.B. Ogale, F. Bai, D. Viehland, Y. Jia, D.G. Schlom, M. Wuttig, A. Roytburd, and R. Ramesh: Multiferroic $BaTiO_3$-$CoFe_2O_4$ nanostructures. *Science* **303**, 661 (2004).
6. J.L. MacManus-Driscoll, P. Zerrer, H.Y. Wang, H. Yang, J. Yoon, A. Fouchet, R. Yu, M.G. Blamire, and Q.X. Jia: Strain control and spontaneous phase ordering in vertical nanocomposite heteroepitaxial thin films. *Nat. Mater.* **7**, 314 (2008).
7. H. Yang, H.Y. Wang, J. Yoon, Y.Q. Wang, M. Jain, D.M. Feldmann, P.C. Dowden, J.L. MacManus-Driscoll, and Q.X. Jia: Vertical interface effect on the physical properties of self-assembled nanocomposite epitaxial films. *Adv. Mater.* **21**, 3794 (2009).
8. J. Yoon, S. Cho, J.H. Kim, J. Lee, Z.X. Bi, A. Serquis, X.H. Zhang, A. Manthiram, and H.Y. Wang: Vertically aligned nanocomposite thin films as a cathode/electrolyte interface layer for thin-film solid-oxide fuel cells. *Adv. Funct. Mater.* **19**, 3868 (2009).
9. Z.X. Bi, J.H. Lee, H. Yang, Q.X. Jia, J.L. MacManus-Driscoll, and H.Y. Wang: Tunable lattice strain in vertically aligned nanocomposite $(BiFeO_3)_x$:$(Sm_2O_3)_{1-x}$ thin films. *J. Appl. Phys.* **106**, 94309 (2009).
10. A.P. Chen, Z.X. Bi, C.F. Tsai, J. Lee, Q. Su, X.H. Zhang, Q.X. Jia, J.L. MacManus-Driscoll, and H.Y. Wang: Tunable low-field magnetoresistance in $(La_{0.7}Sr_{0.3}MnO_3)_{0.5}$:$(ZnO)_{0.5}$ self-assembled vertically aligned nanocomposite thin films. *Adv. Funct. Mater.* **21**, 2423 (2011).
11. M.K. Wu, J.R. Ashburn, C.J. Torng, P.H. Hor, R.L. Meng, L. Gao, Z.J. Huang, Y.Q. Wang, C.W. Chu: Superconductivity at 93 K in a new mixed-phase Y-Ba-Cu-O compound system at ambient pressure. *Phys. Rev. Lett.* **58**, 908 (1987).
12. S.R. Foltyn, L. Civale, J.L. MacManus-Driscoll, Q.X. Jia, B. Maiorov, H. Wang, and M. Maley: Materials science challenges for high-temperature superconducting wire. *Nat. Mater.* **6**, 631 (2007).
13. S.C. Wimbush, J.H. Durrell, C.F. Tsai, H. Wang, Q.X. Jia, M.G. Blamire, and J.L. MacManus-Driscoll: Enhanced critical current in $YBa_2Cu_3O_{7-\delta}$ thin films through pinning by ferromagnetic $YFeO_3$ nanoparticles. *Supercond. Sci. Technol.* **23**, 45019 (2010).
14. T. Haugan, P.N. Barnes, R. Wheeler, F. Meisenkothen, and M. Sumption: Addition of nanoparticle dispersions to enhance flux pinning of the $YBa_2Cu_3O_{7-x}$ superconductor. *Nature* **430**, 867 (2004).
15. B. Dam, J.M. Huijbregtse, and J.H. Rector: Strong pinning linear defects formed at the coherent growth transition of pulsed-laser-deposited $YBa_2Cu_3O_{7-\delta}$ films. *Phys. Rev. B* **65**, 64528 (2002).
16. J.L. MacManus-Driscoll, S.R. Foltyn, Q.X. Jia, H. Wang, A. Serquis, L. Civale, B. Maiorov, M.E. Hawley, M.P. Maley, and D.E. Peterson: Strongly enhanced current densities in superconducting coated conductors of $YBa_2Cu_3O_{7-x}$+$BaZrO_3$. *Nat. Mater.* **3**, 439 (2004).
17. S.R. Foltyn, H. Wang, L. Civale, Q.X. Jia, P.N. Arendt, B. Maiorov, Y. Li, M.P. Maley, and J.L. MacManus-Driscoll: Overcoming the barrier to 1000 A/cm width superconducting coatings. *Appl. Phys. Lett.* **87**, 162505 (2005).
18. S. Kang, A. Goyal, J. Li, A.A. Gapud, P.M. Martin, L. Heatherly, J.R. Thompson, D.K. Christen, F.A. List, M. Paranthaman, and D.F. Lee: High-performance high-T_c superconducting wires. *Science* **311**, 1911 (2006).
19. C.V. Varanasi, J. Burke, L. Brunke, H. Wang, M. Sumption, and P.N. Barnes: Enhancement and angular dependence of transport critical current density in pulsed laser deposited $YBa_2Cu_3O_{7-x}$+$BaSnO_3$ films in applied magnetic fields. *J. Appl. Phys.* **102**, 63909 (2007).
20. C.V. Varanasi, J. Burke, L. Brunke, H. Wang, J.H. Lee, and P.N. Barnes: Critical current density and microstructure variations in $YBa_2Cu_3O_{7-x}$+$BaSnO_3$ films with different concentrations of $BaSnO_3$. *J. Mater. Res.* **23**, 3363 (2008).
21. S.H. Wee, A. Goyal, E.D. Specht, C. Cantoni, Y.L. Zuev, V. Selvamanickam, and S. Cook: Enhanced flux pinning and critical current density via incorporation of self-assembled rare-earth barium tantalate nanocolumns within $YBa_2Cu_3O_{7-\delta}$ films. *Phys. Rev. B* **81**, 140503 (2010).
22. S.H. Wee, A. Goyal, Y.L. Zuev, C. Cantoni, V. Selvamanickam, and E.D. Specht: Formation of, double-perovskite, nanocolumns and their contribution to flux-pinning and J_c in Nb-doped $YBa_2Cu_3O_{7-\delta}$ films. *Appl. Phys. Express* **3**, 023101 (2010).
23. C. Cantoni, Y.F. Gao, S.H. Wee, E.D. Specht, J. Gazquez, J.Y. Meng, S.J. Pennycook, and A. Goyal: Strain-driven oxygen deficiency in self-assembled, nanostructured, composite oxide films. *ACS Nano* **5**, 4783 (2011).
24. H.Y. Wang and J. Wang: Interfacial defects and flux-pinning effects in nanostructured $YBa_2Cu_3O_{7-\delta}$ thin films. *IEEE Trans. Appl. Supercond.* **19**, 3395 (2009).
25. P.N. Barnes, T.J. Haugan, C.V. Varanasi, and T.A. Campbell: Flux pinning behavior of incomplete multilayered lattice structures in $YBa_2Cu_3O_{7-\delta}$. *Appl. Phys. Lett.* **85**, 4088 (2004).
26. W.L. Winterbottom: Equilibrium shape of a small particle in contact with a foreign substrate. *Acta Metall.* **15**, 303 (1967).
27. P. Mele, K. Matsumoto, T. Horide, A. Ichinose, M. Mukaida, Y. Yoshida, S. Horii, and R. Kita: Ultra-high flux pinning properties of $BaMO_3$-doped $YBa_2Cu_3O_{7-x}$ thin films (M = Zr, Sn). *Supercond. Sci. Technol.* **21**, 32002 (2008).
28. A. Ichinose, P. Mele, T. Horide, K. Matsumoto, G. Goto, M. Mukaida, R. Kita, Y. Yoshida, and S. Horii: Microstructures of $REBa_2Cu_3O_y$ adding $BaZrO_3$ or $BaSnO_3$. *Physica C* **468**, 1627 (2008).
29. J. Narayan and B.C. Larson: Domain epitaxy: A unified paradigm for thin film growth. *J. Appl. Phys.* **93**, 278 (2003).
30. M.G. Blamire, J.L. MacManus-Driscoll, N.D. Mathur, and Z.H. Barber: The materials science of functional oxide thin films. *Adv. Mater.* **21**, 3827 (2009).
31. S.R. Foltyn, H. Wang, L. Civale, B. Maiorov, and Q.X. Jia: The role of interfacial defects in enhancing the critical current density of $YBa_2Cu_3O_{7-\delta}$ coatings. *Supercond. Sci. Technol.* **22**, 125002 (2009).

https://doi.org/10.1557/jmr.2012.125 Published online by Cambridge University Press